

II.4.2 Development of Low-Irreversibility Engines

Investigators

C.F. Edwards, Associate Professor, Mechanical Engineering; K.-Y. Teh, S.L. Miller, P.A. Caton, Graduate Researchers

Introduction

In the most general sense of the word, an *engine* is a device that converts heat or chemical energy into work. The most work that can be developed by a particular engine design is its *reversible* work. The *irreversibility* of an engine is the difference between the reversible work that it could develop and the actual work that it performs; it is the lost work. In this research we investigate the potential to design and implement engines with significantly reduced irreversibility, and thereby, improved efficiency.

The relevance of this work to the objective of GCEP is that significant improvements in efficiency are one of the most effective approaches to reducing greenhouse-gas emissions. Since the approach we take is fundamental and comprehensive, it enables improvements both with existing fuels (hydrocarbons) as well as with possible future fuels (e.g. hydrogen).

Background

Improvement of engine efficiency requires efforts in two areas: design and implementation. By design we mean the basic operating cycle or strategy of the engine (e.g., Brayton vs. Stirling cycle). By implementation we mean the degree of perfection with which the design is realized in practice (e.g., the degree to which gas expansion is isentropic). Our focus is on the former (design) aspect. It is based on the realization that current internal combustion engines—gasoline, Diesel, and gas turbine—have been developed based upon an incorrect premise: that they are subject to limitations based on Carnot efficiency. This misconception persists because these engines are often modeled as heat engines (which are subject to Carnot limitations) where, in fact they are reactive engines that are not subject to Carnot proscriptions.

The Carnot misconception has led to erroneous conclusions about how to design combustion engines. The most serious of these is that it is necessary to make the peak temperature in the cycle as high as possible (to improve the Carnot limit). That this is not correct is confirmed by recent experiences with HCCI engines—engines that achieve higher efficiency than their SI counterparts while reducing the peak temperature [1]. And the ultimate example of both the inapplicability of the Carnot criterion and the benefits of low-temperature reaction is the fuel-cell—a reactive engine with first-law efficiency potential in excess of 90% when operated at low temperatures ($\sim 80^\circ\text{C}$ for a typical PEM system).

But even before the details of an engine design are considered, it is worth investigating the work potential of the resource that is to be utilized by the engine. This is the *available energy* or *exergy* of the resource. The exergy of a chemical resource is found by permitting heat and work to be exchanged between the resource and its environment, and by permitting diffusive and reactive interactions between the two. The reversible work that can be achieved under these most-general conditions *is* the exergy, and its value is given by the expression

$$X = (U + P_oV - T_oS) - G_o - \Delta G_{rxn}^o$$

(See reference [2] for a comprehensive discussion of exergy.) This indicates that the absolute upper bound on the work that can be achieved from a resource is dependent upon the both the thermal state of the resource and environment (the first set of terms in parentheses) and on the respective chemical states (the last two terms containing the Gibbs function). For the usual case of a chemical resource that is in thermal and mechanical equilibrium with the environment, it this last term—the change of Gibbs function upon reaction evaluated at the conditions of the environment—that determines its work potential.

Unfortunately, it has proven difficult to construct engines which come close to extracting this limiting amount of work. This is due to a number of complications including the inability to produce perfect devices (turbines, membranes, catalysts) and the inability to produce devices without ancillary complications (e.g., water management in PEM membranes, ionic conductivity in SOFC membranes) that force design choices that are non-optimal (e.g., operation of a fuel cell at elevated temperatures). These later complications often lead to engine designs with what are referred to as *option losses*—reductions in the reversible work potential from the exergy limit by design. In this case, even if perfect devices are realized to implement the design, the work developed will be less than the exergy limit since the design does not take advantage of all possible interactions with the environment. Analysis of specific designs to determine their reversible-work capabilities is the subject of Second-Law Analysis.

It is in this domain—between the bounds of what is possible from an exergy standpoint and those of conventional engine cycles—that we seek to improve engine performance. Stated another way, we propose to improve reactive engine performance by seeking engine designs that reduce design-associated irreversibility. This is accomplished by branching off from the exergy analysis to include selective interactions between the engine and the environment and to consider how these may be implemented in a mathematically optimal fashion. Note that this is in contrast with second-law analysis which seeks improvements in an existing design by reducing implementation irreversibilities. Here we seek improvements by optimal designs within the limitations of allowed interactions. In short it is our objective to bridge between exergy and second-law analysis to produce new design concepts for engines with minimal option-loss irreversibility.

Results

During this past year, our effort has focused on three aspects of low-irreversibility engines:

- (1) experimental studies of achieving improved efficiency in piston engines through use of late-phase combustion,
- (2) computational and analytical studies of adiabatic expansion-engine combustion in order to define optimal design criteria, and
- (3) analysis of isothermal electrochemical engine (fuel cell) operation in order to develop a counterpart non-electrochemical, isothermal expansion engine.

Each of these topics will be discussed separately below.

Results from Late-Phase Combustion Experiments

Late-phase HCCI combustion shows promise as one means to implement a low-irreversibility engine. The basic premise is that by combining the combustion and expansion processes, energy may be extracted during the combustion process and overall losses may be reduced. This is in some ways analogous to a fuel cell in that since energy is extracted in the process of reaction, peak temperatures are held at much lower values than traditional devices, and entropy generation is correspondingly reduced.

The studies undertaken utilize a single cylinder, variable compression ratio engine equipped with variable valve actuation (VVA) as depicted in Figure 1. The use of VVA permits us to tailor the composition and thermal state of the gases in the cylinder by mixing controlled amounts of hot, burned gases (from the previous combustion cycle) with the fresh air-fuel charge. In doing so, the engine can be made to operate as either a spark-ignition (SI) engine or a homogeneous-charge, compression-ignition (HCCI) engine. Both the engine/VVA system and previous HCCI results are described in detail in reference [1].

The late-phase studies undertaken for this project were performed using optimal conditions as determined from our previous work. Propane was chosen as the fuel so as to provide typical hydrocarbon kinetics but without the possibility of inhomogeneity inherent in liquid fueled engines. It was premixed with the air well ahead (~1 m) of the engine to insure a homogeneous charge. The equivalence ratio was held at 0.95—a value corresponding to optimum operation in our previous tests. Compression ratio was set to 15:1—a value high enough to provide a broad range of HCCI operation but low enough to avoid excessive heat losses.

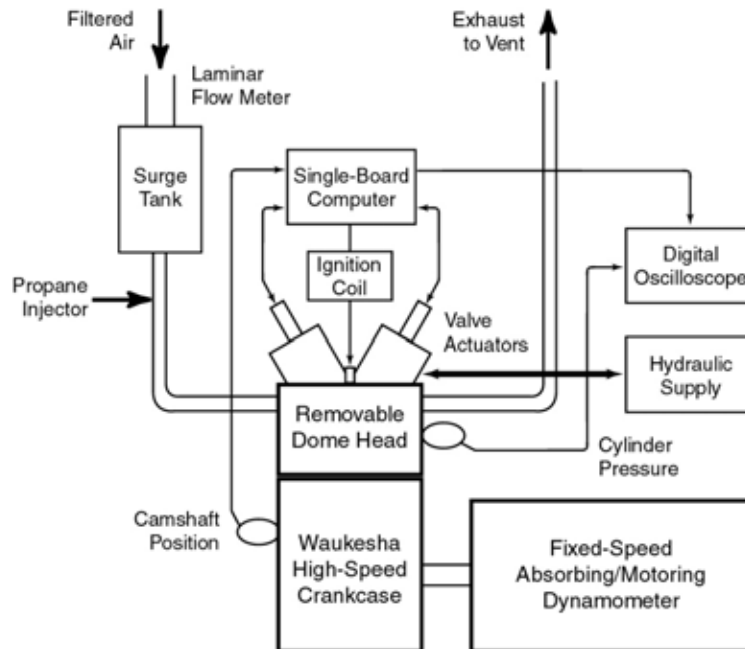


Figure 1: Engine used to study late-phase combustion. Closed-loop, fully flexible electrohydraulic valve actuation is used to enable exhaust reinduction for initiating late-phase HCCI. In-cylinder pressure and exhaust emissions are used to determine indicated engine performance metrics.

Two sets of intake valve profiles were used to enact late phase combustion. In this first set, the intake valve was opened at its nominal (SI) opening time, held at full lift, but then closed prematurely (as required to obtain late phasing). In the second set, the intake valve was held open throughout its nominal (SI) period, but the lift was reduced to adjust phasing. In both cases, the exhaust valve was held open throughout the intake stroke (as in our previous studies) so that by adjusting the intake valve alone the residual fraction (mass fraction of burned gas) could be varied.

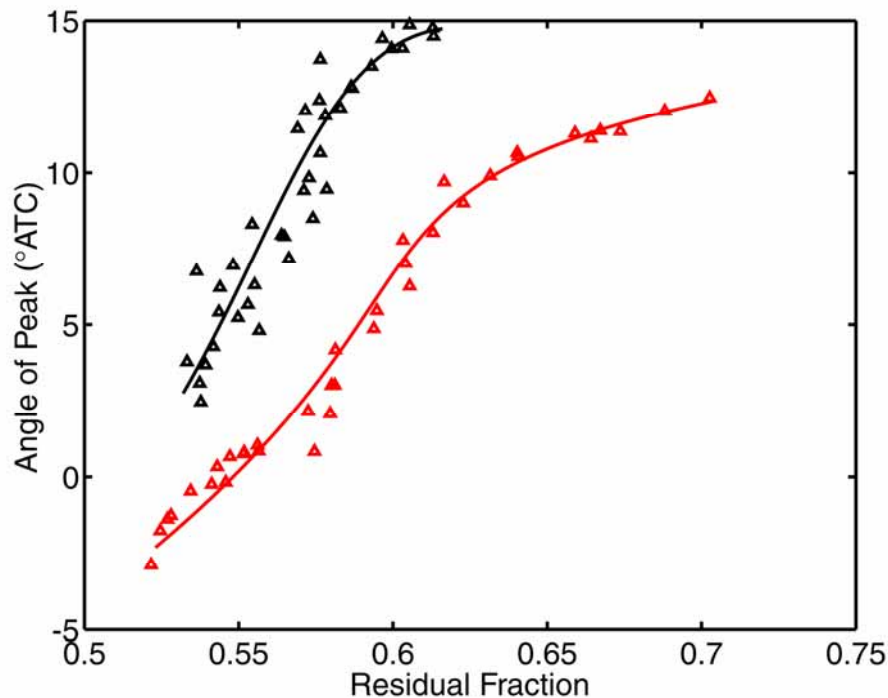


Figure 2: Effect of residual fraction on phasing of HCCI combustion as indicated by the crank angle at which peak pressure occurs. The black line corresponds to full-lift, partial-duration intake valve profiles. The red line is from full-duration, partial-lift profiles.

As illustrated in Fig. 2, both sets of valve profiles were capable of initiating combustion with phasing after top dead center (ATC). The full-duration, partial-lift strategy was capable of achieving a wider range of residual mass fractions, but the partial-duration, full-lift strategy was able to achieve overall later combustion timings. Note that in either case, increasing the residual fraction causes an increase in the extent to which combustion can be delayed. (Preliminary studies have been conducted which attempt to isolate the effects of late phasing from those of residual fraction, but these are not yet complete and so will be reported at a future date.)

Figure 3 shows the effect of combustion phasing on the indicated thermal efficiency of the cycle. Regardless of the strategy employed, delaying combustion into the expansion process enables a significant increase in efficiency. As phasing is delayed from top center to $\sim 15^\circ$ ATC efficiency rises from $\sim 30\%$ to $\sim 43\%$. At a given combustion phasing, some differences due to the choice of valve profiles are evident, but these are generally smaller effects than the overall change with phasing. (The reasons for these differences are currently under investigation.)

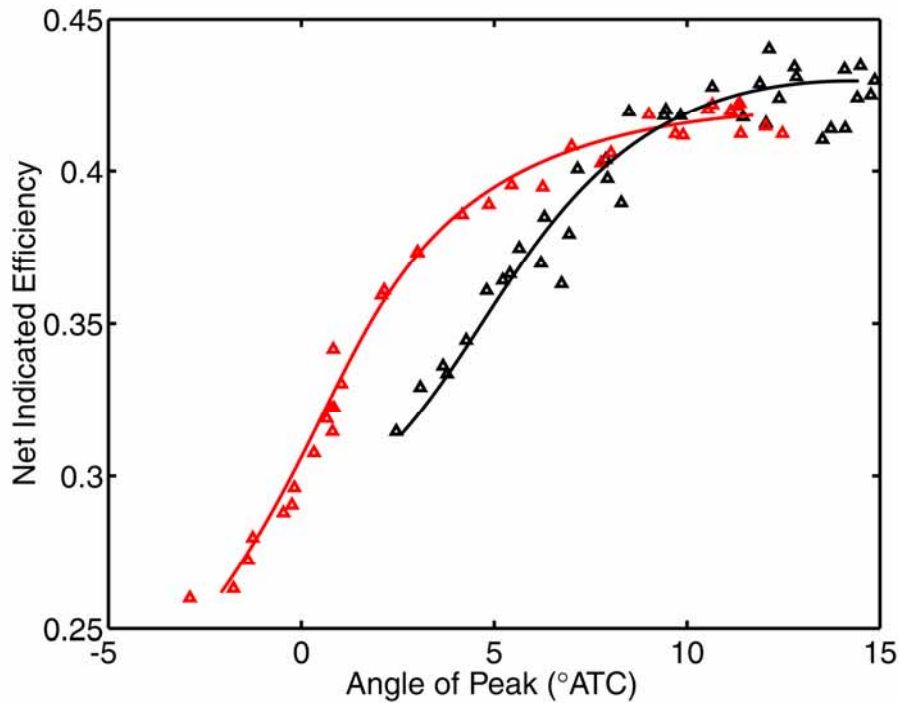


Figure 3: Effect of combustion phasing on indicated thermal efficiency. The black line corresponds to full-lift, partial-duration intake valve profiles. The red line is from full-duration, partial-lift profiles.

Figure 4 shows the effect of combustion phasing on exhaust temperature as measured immediately downstream of the exhaust port. For clarity, only data from the full-lift, partial duration tests are shown. The indicated thermal efficiency is also plotted for comparison. These data indicate that the rise in efficiency does not come at the expense of the exhaust enthalpy. This is consistent with a hypothesis that since the combustion has been delayed, some of the ability to extract energy via expansion work has been lost. The results are inconsistent with the hypothesis that delaying combustion can reduce irreversibility without the occurrence of other effects.

Figure 5 resolves the inconsistencies by showing that the increase in efficiency is due to a drastic reduction in heat losses. Although our objective in studying late-phase combustion has been to reduce *combustion* irreversibility, these results show that the single biggest effect is to reduce overall heat losses (and their concomitant irreversibility) from the system. This reduction stems from having lowered the peak temperature in the cylinder (by late phasing) such that the driving potential for losses is significantly reduced. An additional component of this reduction may be a reduced convective heat transfer rate due to reduced turbulence (laminarization) during the expansion stroke. Modeling studies of the heat transfer during HCCI combustion are currently underway.

Taken in combination, Figs. 4 and 5 suggest that the potential for improving efficiency via late-phase HCCI combustion is greater than thought previously. This is because the gases have still not undergone optimal expansion. Using VVA, where the compression and expansion ratios can be set independently, the exhaust gases may be expanded further. Studies to investigate the potential of optimal expansion are planned.

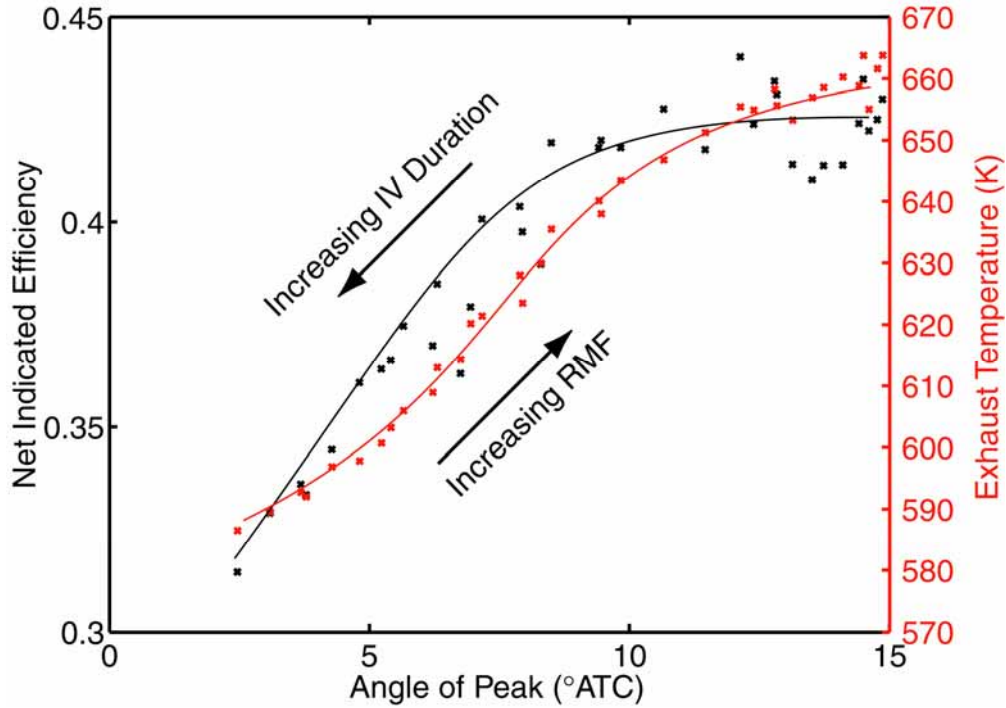


Figure 4: Comparison of the effect of combustion phasing on efficiency and exhaust temperature. Only results for full-lift, partial-duration intake valve profiles are shown.

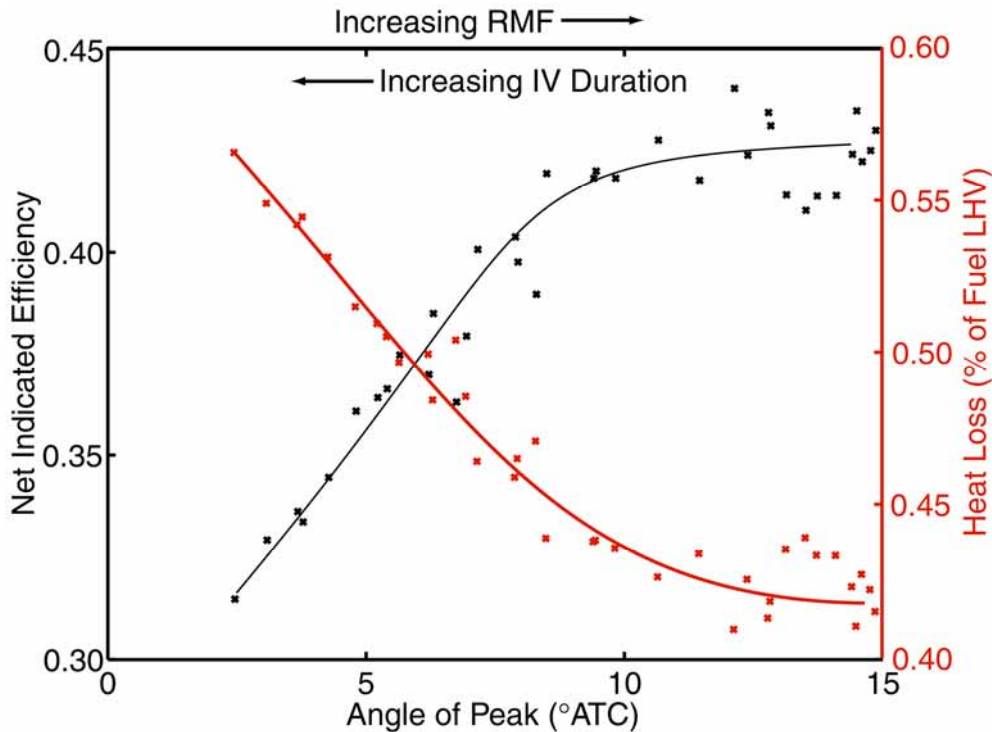


Figure 5: Comparison of the effect of combustion phasing on efficiency and heat transfer losses. Only results for full-lift, partial-duration intake valve profiles are shown.

Figure 6 confirms that the reduction of heat loss using late-phase combustion is not peculiar to the full-lift, partial-duration valving strategy. Essentially similar results are obtained with either strategy at a fixed combustion phasing.

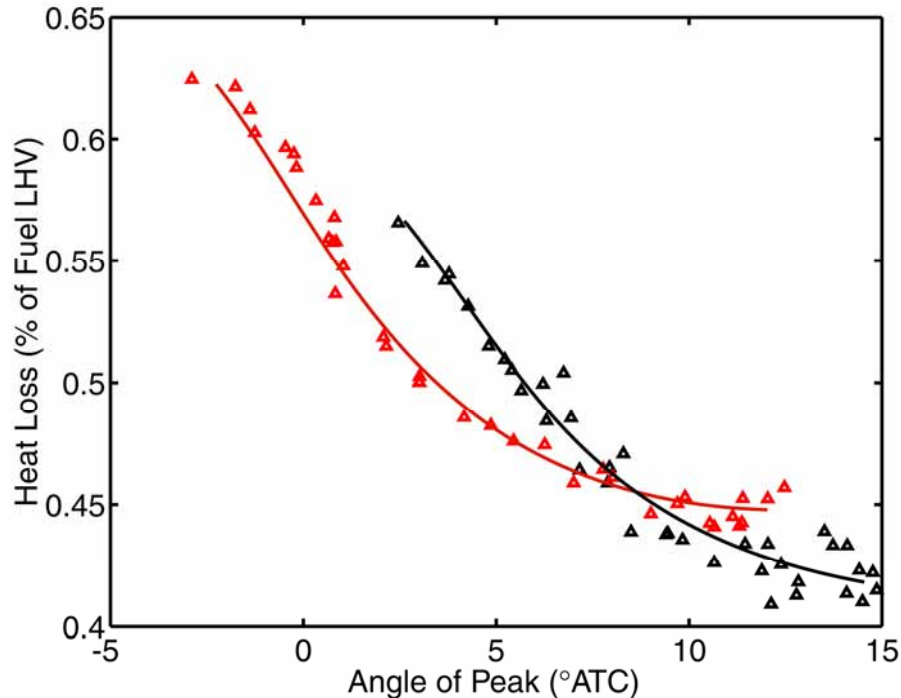


Figure 6: Effect of combustion phasing on heat loss for both sets of valve profiles. The black line corresponds to full-lift, partial-duration intake valve profiles. The red line is from full-duration, partial-lift profiles.

Results from Simulation and Analysis of Adiabatic Expansion Engines

In these studies we investigate the possibility of reducing the irreversibility of combustion engines by extracting work during an *adiabatic* combustion process. The question posed is whether, by suitable choice of the volume-time profile, the combustion and work-extraction (expansion) processes can be combined in an optimal fashion to improve efficiency. In keeping with our ideal design investigations, the analyses are performed assuming an adiabatic enclosure. While the experimental results show that this is not what happens in experiments, this analysis provides a key stepping stone in understanding what is possible in an optimal-design sense. It is also important for understanding what is happening in the engine tests, since in the experiments the effects of heat transfer and reduction of combustion irreversibility cannot be deconvolved. (Analytical studies incorporating the effects of heat transfer are planned for future work.)

Simulation Procedure

The simulations are performed using Cantera, an open-source program for chemical kinetics and thermodynamic simulations, in conjunction with the suite of ODE solvers available in MATLAB. The GRI-Mech 3.0 combustion reaction mechanism and its thermochemical database are used in the analysis. Since the combustion mode under

consideration is homogeneous-charge compression ignition, a zero-dimensional model is used; effects of spatial inhomogeneities are not considered.

The process analyzed is based on the slider-crank motion of a reciprocating engine (compression ratio 13:1; ratio of connecting rod length to crank radius 5.52:1) operating at 1800 RPM. Starting with a fuel/oxidizer mixture at bottom dead center (BDC), the compression stroke, carried out adiabatically, raises the mixture temperature and initiates chemical reaction. Under these conditions, a stoichiometric mixture of hydrogen/air diluted by 40% (by mass) of combustion products (water and nitrogen) initially at 425 K, 1 atm is predicted to autoignite at 10°ATC (crank angle degrees after top center). The product gas mixture, at elevated pressure, expands during the power stroke and delivers expansion work to the piston.

To simulate work extraction during the combustion process, the slider-crank motion is modified by varying the speed with which it is executed during the expansion stroke (the compression process remains unchanged). While this motion clearly defies the constraints of real reciprocating engines (as does our assumption of an adiabatic process), it nevertheless provides a simple model by which the feasibility of optimizing combustion via work extraction can be investigated.

Results for Hydrogen-Air Combustion

Figure 7 shows representative pressure and temperature profiles generated from the simulation for increasing piston speed during the expansion stroke. While Fig. 7.a and 7.b show rapid pressure and temperature rises associated with the homogeneous charge combustion model, the peak pressure and temperature decrease with increasing speed of expansion. A higher speed of expansion, corresponding to more rapid work extraction while the combustion is occurring, also leads to a delay in initiation of the combustion process.

Figure 7.c showing pressure and temperature rise near 45°ATC (for an expansion speed of 2288 RPM) is a result of the adiabatic assumption used in the model. The gas mixture temperature remains near 1000 K for an extended period of time while no energy is lost by heat transfer. During this time the pool of reactive radical species is built up instead of depleted, as wall destruction of radicals is not included in the model. The result is the occurrence of combustion far beyond TDC which we would not expect in practice. But this case does help to illustrate the nonlinearity of the combustion process since it depicts how the results change from mild-but-complete combustion at 2288 RPM (Fig. 7.c) to incomplete combustion at 2290 RPM (Fig. 7.d).

Figure 7 shows that work extraction during combustion, by speeding up the expansion stroke of the engine, can partially “restrain” combustion, delaying it and lowering the peak temperature and pressure. However, this is done at the expense of completing the rest of the reaction at a lower temperature and pressure. As a result, the total entropy generated actually increases, as shown on the internal energy-entropy diagram of Fig. 8.

The trend of increasing entropy generation continues until a critical engine speed is attained. Expansion rates beyond this critical speed are too fast for the combustion to go to completion, resulting in a quenched reaction (Fig. 7.d). Consequently, the locus of final u, s values for the gas mixture at the end of the power stroke, shown in black in Fig. 8, veers away from the equilibrium product line (red).

II.4 Project Results: Advanced Combustion

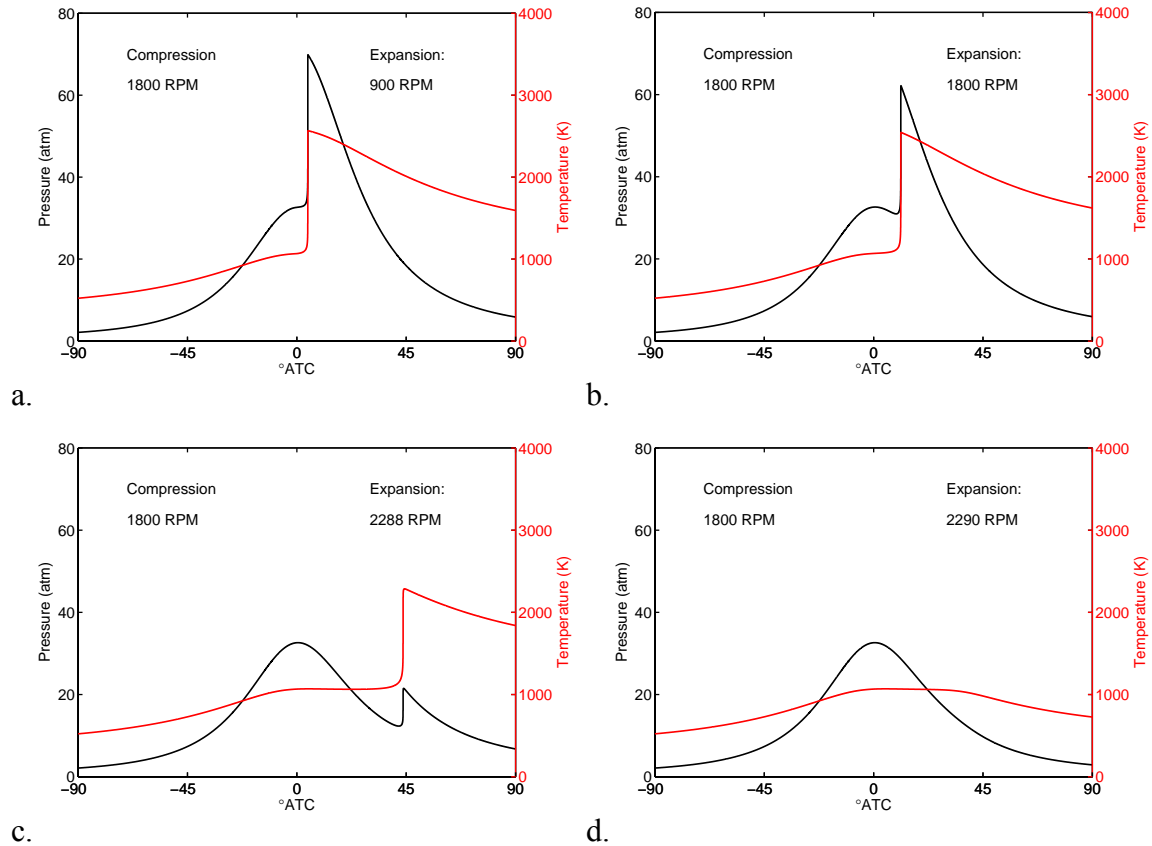


Figure 7: Pressure and temperature profiles for dilute H_2 /air combustion at four speeds during expansion: a. 900; b. 1800; c. 2288; and d. 2290 RPM respectively.

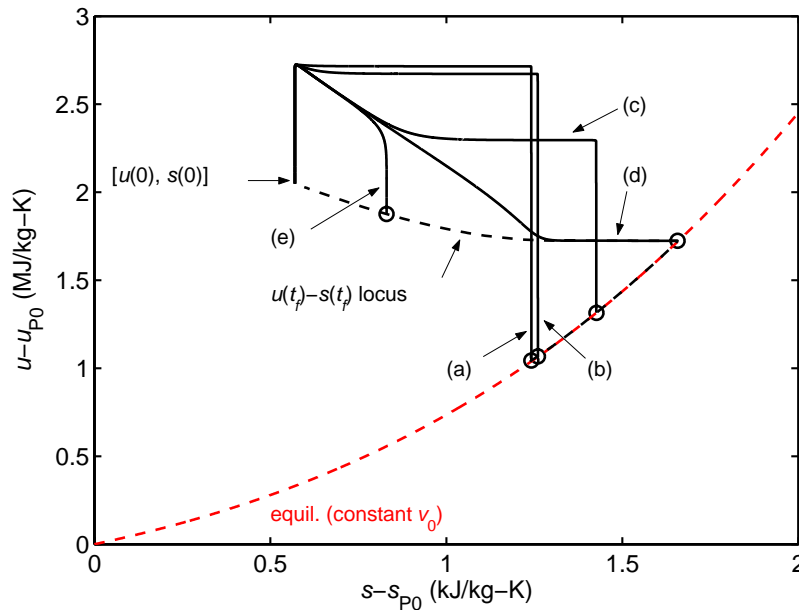


Figure 8: u - s diagram for dilute H_2 /air combustion at expansion speeds of a. 900; b. 1800; c. 2288; d. 2288.5; and e. 2290 RPM respectively. The locus of final u, s values (black, dotted) shows higher entropy or incomplete combustion when work is extracted during reaction. The lowest entropy generation is for constant-volume combustion.

Besides considering the net amount of work output (which, for an adiabatic system, equals the net difference in internal energy from the start of compression u_0 to the end of expansion u_f), an alternative measure of the efficiency of energy utilization is to compare the work output to the exergy decrease during the process. This ratio is termed the *extent of exergy utilization*, and is denoted η_x

$$\eta_x = \frac{u_0 - u_f}{x_0 - x_f} \quad (1)$$

A utilization indicates efficient conversion of the exergy to useful work. Figure 9 shows η_x versus s for the end states of the cases discussed above.

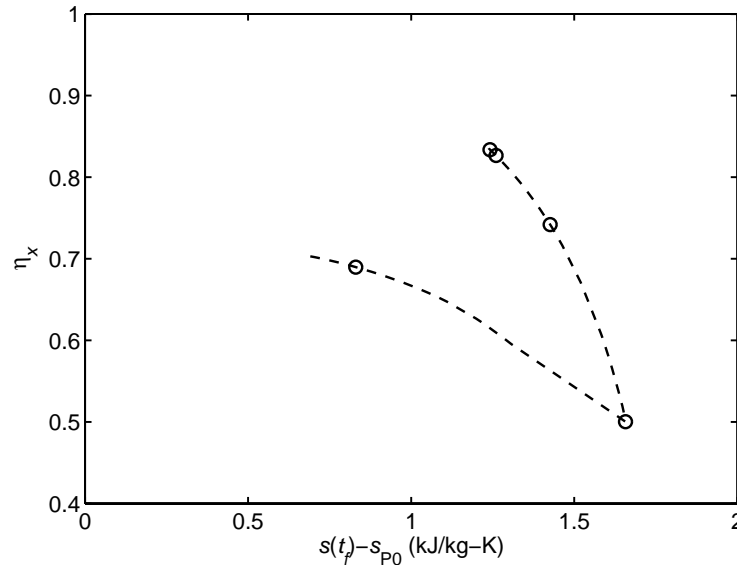


Figure 9: Extent of exergy utilization η_x versus entropy s for the gas mixture at the end of the expansion stroke. The circles correspond to simulations at the five expansion speeds depicted in Fig. 8.

In Fig. 9 we see that combustion without work extraction remains the most efficient design. Increasing expansion speed reduces η_x until it reaches a minimum at the critical speed discussed above, which corresponds to maximum entropy generation. The lower branch of the η_x - s plot corresponds to rapid expansions that lead to quenched reactions. In this case, some fuel remains after the power stroke and is still available for utilization in a subsequent process. While the net amount of work output is smaller with increasing speed (see Fig. 2), the corresponding amount of exergy destroyed also decreases, leading to higher η_x , although it never exceeds the case for slow expansion and near-constant volume combustion.

Results for Methane-, Propane-, and Methanol-Air Combustion

Similar results are obtained when, instead of hydrogen, simple hydrocarbons and methanol are used as a fuel. Figure 10 shows the simulation results, summarized on u - s diagrams, for combustion of methane, propane, and methanol.

II.4 Project Results: Advanced Combustion

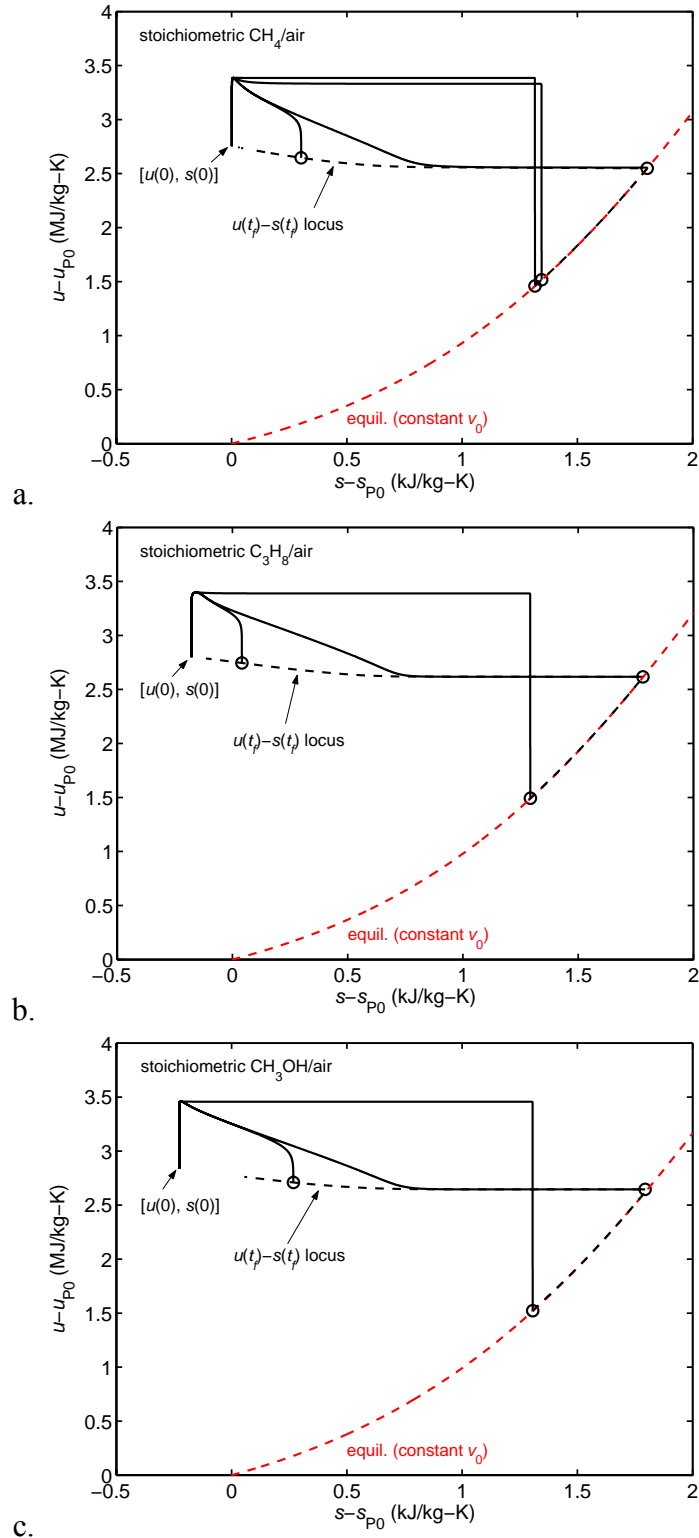


Figure 10: $u-s$ diagrams for reaction of a. methane; b. propane; and, c. methanol at several engine expansion speeds, leading to complete, mild-but-complete, and incomplete combustion. The trends are similar to that for hydrogen (c.f. Fig. 8): higher entropy generation and/or incomplete combustion when energy is extracted during reaction.

For each set of simulations, the initial conditions are chosen such that, with the engine operating at 1800 RPM, the fuel/air mixture would autoignite soon after TDC. Unlike hydrogen/air combustion, however, the early part of the compression stroke in hydrocarbon combustion engine is spent in pyrolyzing the fuel, before the oxy-hydrogen reaction mechanism takes over to build up the radical pool for ignition. This delay in ignition can be compensated for by using significantly less dilute fuel/air mixture at higher initial mixture temperature to facilitate thermal decomposition.

The simulations shown on Fig. 10 assume the initial fuel/air mixture is at stoichiometric proportions *without* dilution. The initial gas pressure is 1 atm. Table 1 lists the initial gas temperatures assumed for the different fuels.

Table 1. Initial gas mixture temperatures used in simulations.
Dilution is assumed in H₂/air combustion only.

| Fuel | T_0 (K) |
|--|-----------|
| H ₂ (diluted by 40% mass of products) | 425 |
| CH ₄ | 525 |
| C ₃ H ₈ | 550 |
| CH ₃ OH | 575 |

Adiabatic, Reactive Engine Optimization

From the simulation results presented in the previous section, it can be seen that any attempt to extract work while the combustion reaction is underway actually *reduces* the overall work output of the system. While this conclusion is not comprehensive—it can only be stated as true for the conditions and fuels investigated—it is counter-intuitive and, in fact, opposite to our original, fuel-cell-motivated hypothesis. For this reason, an analytical optimization study was undertaken to test the opposite hypothesis: that for an adiabatic, reactive engine, optimum efficiency occurs when combustion is conducted under constant-volume conditions, regardless of the dynamics of the process. As shown below, this latter hypothesis is correct—one necessary condition for optimal adiabatic combustion is that it occurs at constant (minimum) volume—in agreement with the results of the previous simulations.

The discussion is divided into three sections: the mathematics of constrained system optimization; optimization of the adiabatic, reactive engine system; and the conclusions drawn from the study.

Optimization of Constrained Systems

Consider an autonomous dynamic system whose state $x:[0, t_f] \rightarrow R^n$ is described by the ordinary differential equations

$$\dot{x}_i(t) = f_i(x(t), u(t)), \quad i = 1, \dots, n \quad (2)$$

where $u:[0, t_f] \rightarrow R^m$ is the input to the system which can be controlled or modified. Given some initial state $x(0) = x_0$, prescribing $u(t)$ as a function of time over the interval $0 \leq t \leq t_f$ uniquely determines the evolution of the system over that time interval.

The goal of the optimization process is to modify $u(t)$ such that the trajectory of system (2) maximizes the functional

$$J = \int_0^{t_f} F(x(t), u(t)) dt \quad (3)$$

subject to various types of constraints. Table 2 lists three types of constraints relevant to the adiabatic piston engine problem at hand.

Table 2: Types of constraints in adiabatic piston engine optimization problem.

| Constraint type | Notation | Eqn. |
|-------------------------------------|---|-------|
| Final state constraints | $x_i(t_f) = (x_f)_i, \quad i = 1, \dots, p < n$ | (4.a) |
| Control input inequality constraint | $g(u(t)) \geq 0$ | (4.b) |
| State inequality constraint | $h(x(t)) \geq 0$ | (4.c) |

Constraints of the form (4.b,c) place the optimization problem outside the scope of classical calculus of variations. Using topological arguments, Pontryagin *et. al.* [3] derived the Maximum Principle, which provides the necessary optimality conditions for such problems. Alternatively, geometrical concepts such as limiting surfaces can also be used to derive the conditions (see Ref. [4]). Hartl *et. al.* [5] reviewed various forms of the Maximum Principle for problems with state-variable inequality constraints.

One form of the Maximum Principle is presented here in brief, for the specific case of (1) a single input $u: [0, t_f] \rightarrow R$, i.e. $m = 1$, and (2) a single state constraint (4.c) of order 1. This means u explicitly appears after $h(x)$ is differentiated once with respect to t .

Constraint (4.c) is assumed *active* (i.e. $h(x) = 0$) on the time interval $t \in [\tau_1, \tau_2] \subset [0, t_f]$ which is mathematically equivalent to the pair of constraints

$$\dot{h}(x, u) = 0 \quad \forall t \in [\tau_1, \tau_2] \quad (4.c-i)$$

$$h(x(\tau_2)) = 0 \quad (4.c-ii)$$

In fact, equation (4.c-ii) can be evaluated at any time $t \in [\tau_1, \tau_2]$ although evaluations at $t = \tau_1$ (the so-called *entry time*) or τ_2 (the *exit time*) are most common.

When constraint $h(x)$ is active, equation (4.c-i) also imposes an additional restriction on the set of admissible inputs originally defined by (4.b). Define this set Ω'

$$\Omega'(x) = \{u : g(u) \geq 0, \dot{h}(x, u) = 0 \text{ if } h(x) = 0\} \quad (5)$$

Define the variational Hamiltonian H

$$H(x, u, \lambda) = F(x, u) + \sum_k \lambda_k f_k(x, u) \quad (6)$$

where λ_i is the co-state corresponding to state x_i . The state and co-state dynamics can then be expressed in terms of H

$$\dot{x}_i = \frac{\partial H}{\partial \lambda_i} \quad (7.a)$$

$$\dot{\lambda}_i = -\frac{\partial(H + v\dot{h})}{\partial x_i} \quad (7.b)$$

where the state constraint (4.c-i) affects the system dynamics via the multiplier ν .

An optimal solution of the problem stated above must satisfy the following necessary conditions (the asterisks denote optimal input, states, and co-states):

$$H(x^*, \lambda^*, u^*) = \sup_{u \in \Omega'} H(x^*, \lambda^*, u) = 0 \quad \forall t \in [0, t_f] \quad (8.a)$$

$$\lambda_i^*(t_f) = 0, \quad i = p+1, \dots, n \quad (8.b)$$

$$\nu \begin{cases} = 0 & \text{if } h(x) > 0 \\ \geq 0 & \text{if } h(x) = 0 \end{cases} \quad (8.c)$$

$$\lambda^*(\tau_2^-) = \lambda^*(\tau_2^+) + \nu(\tau_2) \nabla h(x^*(\tau_2)) \quad (8.d)$$

Equations (8.a) is akin to the Euler-Lagrange equations from calculus of variations. Equation (8.b), a specific form of the *transversality condition*, means that the co-state λ_i^* has to vanish at time t_f unless the corresponding final state $x_i(t_f)$ is prescribed. Equations (8.c,d) impose the constraints (4.c-i,ii). Pontryagin called the discontinuity on co-state trajectories (8.d) an *exit jump condition*. As discussed above, the equivalent *entry* jump condition can be derived if (4.c-ii) is evaluated at $t = \tau_1$ instead.

The Maximum Principle as stated above provides necessary optimality conditions without fixing final time t_f . The solution for fixed-time problems is readily obtained by introducing a new state $x_{n+1} \equiv t$ with dynamics $\dot{x}_{n+1} = 1$, initial and final state $x_{n+1}(0) = 0$, $x_{n+1}(t_f) = t_f$; the necessary conditions (8.a-d) remain unchanged.

This technique is also applicable to the optimization of non-autonomous systems.

The necessary conditions (8.a-d) result in a multi-point—at times $t = 0$, t_f and one or more exit times τ_2 's—boundary value problem involving the ordinary differential equations (7.a,b). One major complication is that the optimal number of switches between constrained and unconstrained system trajectories, as well as the optimal switching times, are not known a priori. Numerical methods based on nonlinear programming are often used to solve for inputs satisfying the necessary conditions of the Maximum Principle (see Ref. [6] for an overview). However, most nonlinear programming techniques are only capable of finding local minima (and maxima) by estimating local gradient and curvature iteratively. Nonlinear constrained optimization in the global sense remains an active area of research.

It is also important to keep in mind that the Maximum Principle is generally not constructive. It provides the necessary conditions that the optimal system input must satisfy. However, an input that is constructed to satisfy all the conditions may turn out to be non-optimal. Sufficiency and uniqueness conditions based on the Maximum Principle often rely on Hamiltonian concavity (see Ref. [5] for details).

Optimization of Piston Motion for an Adiabatic, Reactive Engine

In order to understand our experimental and simulation results, the Maximum Principle was applied to the problem of optimizing the piston motion of an adiabatic, chemically reactive engine for maximum expansion-work output. The gas in the cylinder

11.4 Project Results: Advanced Combustion

is modeled as a homogeneous, ideal-gas mixture. Its thermodynamic state¹ at any time t is defined by the properties:

- v = specific volume of the gas, and hence of the piston cylinder;
- Y = mass fractions of all m chemical species in the gas mixture (an m -vector)²;
- T = gas temperature.

The system dynamics are thus

$$\dot{v} = w \quad (10.a)$$

$$\dot{Y}_i = f_i(v, Y, T), \quad i = 1, \dots, m \quad (10.b)$$

$$\dot{T} = -\frac{\frac{RT}{v} \sum_k \frac{Y_k}{MW_k} w + \sum_k u_k f_k}{\sum_k c_{v_k} Y_k} = f_T(v, Y, T, w) \quad (10.c)$$

Cast as an optimization problem as presented in the previous section, the functional to be maximize is

$$\text{work} = \int_0^{t_f} \frac{RT}{v} \sum_k \frac{Y_k}{MW_k} \cdot w \, dt \quad (11)$$

The input to the system, w , is the rate of volume change for the gas and is taken to be directly proportional to the piston speed (10.a). Chemical kinetics dictate the net production rate of species i , denoted f_i (10.b). For gas-phase reactions due to molecular collisions, f_i is solely a function of the states. Conservation of energy for the adiabatic system then determines the rate of change of the gas temperature, denoted f_T (10.c). f_T depends on the states, but is also a linear function of the input w .

The system is constrained as follows: (1) The time of reaction t_f is fixed. The technique of introducing a new state $\tau \equiv t$ will be used to address this constraint. (2) All initial states are prescribed, with the cylinder restored to its initial volume at time t_f .

$$\begin{aligned} v(0) &= v_0 & v(t_f) &= v_0 \\ Y(0) &= Y_0 \\ T(0) &= T_0 \end{aligned} \quad (12.a)$$

(3) The piston speed is bounded by the (common) maximum compression and expansion speed w_m . Imposing this input constraint makes physical sense, and is also essential for the analytical results below.

$$|w| \leq w_m \quad (12.b)$$

¹ In the dynamical system sense, v , Y and T are the “states” in this system and will be referred to as such in subsequent sections.

² For each species i ($i = 1, \dots, m$) MW_i is its molecular weight, while u_i and c_{v_i} , both functions of T , are its total internal energy (chemical plus sensible) and specific heat at constant volume.

(4) The geometric compression ratio of the engine is fixed at CR . The inequality $v_0/CR \leq v \leq v_0$ is expressed as two state inequality constraints of the form (4.c)

$$\begin{aligned} h_{TC}(v, Y, T) &= v - v_0/CR \geq 0 \\ h_{BC}(v, Y, T) &= v_0 - v \geq 0 \end{aligned} \quad (12.c)$$

For this piston engine optimization problem, the Hamiltonian H is linear with respect to the input w .

$$\begin{aligned} H &= Pw + \lambda_v w + \sum_k \lambda_k f_k + \lambda_T f_T + \lambda_\tau \\ &= \left[\frac{RT}{v} \left(\sum_k \frac{Y_k}{MW_k} \right) \left(1 - \frac{\lambda_T}{\sum_k c_{v_k} Y_k} \right) + \lambda_v \right] \cdot w + \left[\sum_k \lambda_k f_k - \lambda_T \frac{\sum_k u_k f_k}{\sum_k c_{v_k} Y_k} \right] + \lambda_\tau \\ &= H_1(v, Y, T) \cdot w + H_2(v, Y, T) \end{aligned} \quad (13)$$

where the restricted set of admissible input is

$$\Omega' = \{w : |w| \leq w_m, \text{ and } w = 0 \text{ if } v = v_0/CR \text{ or } v_0\} \quad (14)$$

By Equation (8.a) of the Maximum Principle, the optimal input w^* must maximize H . Therefore, w^* can only take on one of three values at any instant $t \in [0, t_f]$:

$$w^*(t) = \arg \sup_{w \in \Omega'} H = \begin{cases} +w_m & \text{if } H_1 > 0, h_{TC, BC} \text{ inactive} \\ -w_m & \text{if } H_1 < 0, h_{TC, BC} \text{ inactive} \\ 0 & \text{if } h_{TC} = 0 \text{ or } h_{BC} = 0 \end{cases} \quad (15)$$

In other words, the optimal piston motion that maximizes the expansion work output is piecewise constant. The piston moves at either maximum compression or expansion speed, depending on the coefficient H_1 of the Hamiltonian (13), *unless* the piston is constrained by the geometric compression ratio of the engine, in which case it remains stationary at TDC or BDC.

Conclusions from this Study

As shown via the Maximum Principle, any piston motion that is not piecewise constant—for instance, the slider-crank motion—does not maximize the expansion work output for an adiabatic, reactive engine. Optimally, the piston would move at either maximum compression or expansion speed, or remain stationary when at TDC or BDC. This is consistent with the simulation results presented above, which indicate that work output of the engine is highest when combustion is allowed to proceed at constant volume near TDC without attempting to extract work during the reaction process. We therefore conclude that adiabatic, constant volume combustion at the minimum allowable volume is *likely* to maximize the piston work output.

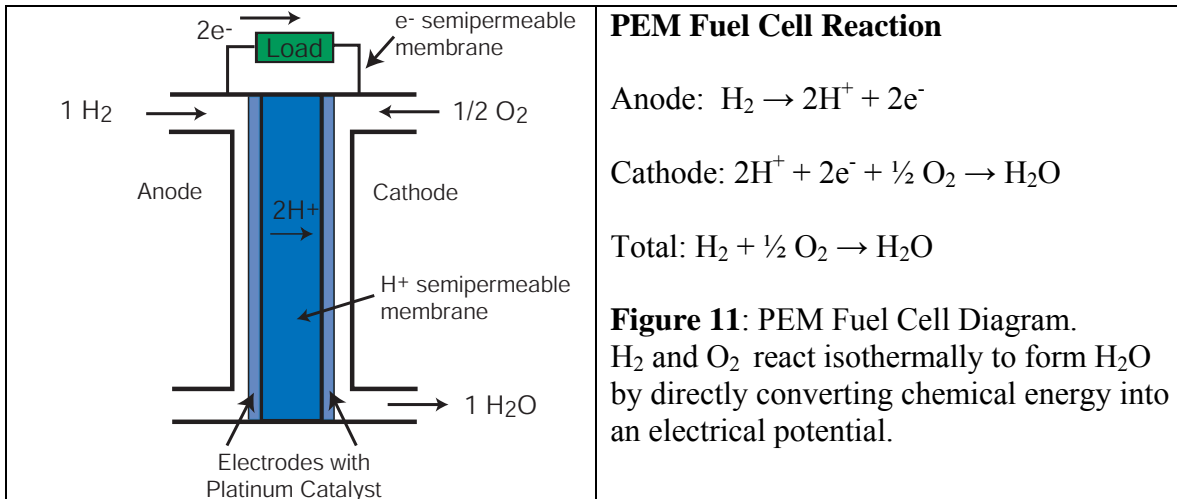
Equally important is the observation that changing the gas phase chemical kinetics would not affect this conclusion, as the Hamiltonian H remains linear with respect to input w (i.e. piston speed). The structure of H changes only if the adiabatic assumption on the system model is abandoned. This is an important and counter-intuitive conclusion.

In effect we have proven that for the overly restrictive adiabatic, reactive expansion case, regardless of dynamics, the optimal solution cannot be obtained by contouring the volume-time profile alone. We also note that the opposite is true—for the less restrictive case with a specified non-linear interaction, we expect that an optimal, non-limit-value solution for the volume-time profile *will* exist. Understanding that optimization problem—in particular the case permitting heat transfer—is one of the next topics that will be addressed in this research.

Results from Analysis of Isothermal Electrochemical and Expansion Engines

Fuel cells are isothermal electrochemical engines that convert chemical energy stored in the bonds of a fuel into electrical work. A PEM (Proton Exchange Membrane) fuel cell uses hydrogen and oxygen as fuel. For every hydrogen molecule consumed, two electrons travel across a potential gradient from the anode to the cathode, producing electrical work. Other work producing devices, specifically combustion engines, first convert chemical energy into sensible energy, raising the overall entropy of the system and therefore, decreasing the theoretical work output. The expansion analogue to the fuel cell, an isothermal device that converts chemical energy directly into a pressure gradient, should have higher theoretical efficiencies than current combustion engines. Our objective in this work is to see if such a reversible expansion engine can be developed.

To understand how this expansion device would work, the fuel cell must be analyzed more closely. A diagram of a PEM fuel cell is shown in Fig. 11. It is composed of two electrodes, each coated with a platinum catalyst surrounding a polymer electrolyte. In a PEM fuel cell, H₂ undergoes dissociative chemisorption onto the platinum catalyst. The electron is pulled into the conduction band by the ionic cores of the platinum, allowing the proton H⁺ to enter the electrolyte. The proton diffuses across the electrolytic semipermeable membrane due to a concentration gradient until it reaches the cathode. At the cathode, the protons combine with the oxygen that is adsorbed onto the cathode’s platinum surface.



The cathode is now at a higher voltage than the anode, creating a positive electrical potential for the electron at the anode. The electron moves to the cathode through its own semipermeable membrane, the conduction band of the metal catalyst and external wiring,

to combine with the proton and oxygen. The water that is formed is drained from the catalyst to maintain the concentration gradients for the reactants. Electrical work is extracted from the electron as it moves across the electrical potential gradient. This work is proportional to the cell potential difference

$$W_{\text{out, max}} = -\Delta G_{\text{tot}} = -\Delta\mu_{\text{tot}} = \mu_{\text{H}_2} + \frac{1}{2}\mu_{\text{O}_2} - \mu_{\text{H}_2\text{O}} = 2F(\phi_{\text{cathode}} - \phi_{\text{anode}})$$

where $W_{\text{out, max}}$ is the maximum work output per mole of H_2 and G is the molar Gibbs free energy which is equal to μ , the chemical potential, F is Faraday's constant, and ϕ is the electrical potential. The two in the last term is required because two moles of electrons flow for every mole of hydrogen consumed. The maximum possible work coincides with the maximum cell potential and occurs theoretically at equilibrium.

An abstract version of the fuel cell diagram is shown in Fig. 12 below next to a similar diagram of the expansion device analogue. Species AB and C are the reactants and enter the device separately at points labeled (1) and (2) on the diagram. These labels replace the "anode" and "cathode" labels on the fuel cell diagram. Specie AB enters the system at (1) and splits into its components A and B. Specie A diffuses to (2) through a semipermeable membrane creating a partial pressure increase in B at (1). Specie B then flows to (2) where it combines with C and A to form the product ABC. In this device the work is extracted from a pressure gradient rather than an electrical potential gradient. Since specie A is diffusing due to a chemical gradient, it might be possible to extract work here as well as from the flow of specie B. The analogy with the fuel cell is consistent with this idea; if a device existed that could extract work from the flow of protons across the electrolyte, work could be extracted in this manner from fuel cells too.

At equilibrium, $\Delta G_{\text{tot}} = \Delta\mu_{\text{tot}} = 0$ at both points (1) and (2) on the device.

$$\Delta\mu_1 = \mu_A + \mu_{B1} - \mu_{AB} = 0; \text{ and}$$

$$\Delta\mu_2 = \mu_{ABC} - \mu_A - \mu_{B2} - \mu_C = 0$$

where μ_i is the chemical potential of specie i . The chemical potential can be written to show its dependence on the partial pressure of specie i

$$\mu_i = \mu_i^\circ(T, P^\circ) + RT\ln(P_i/P^\circ)$$

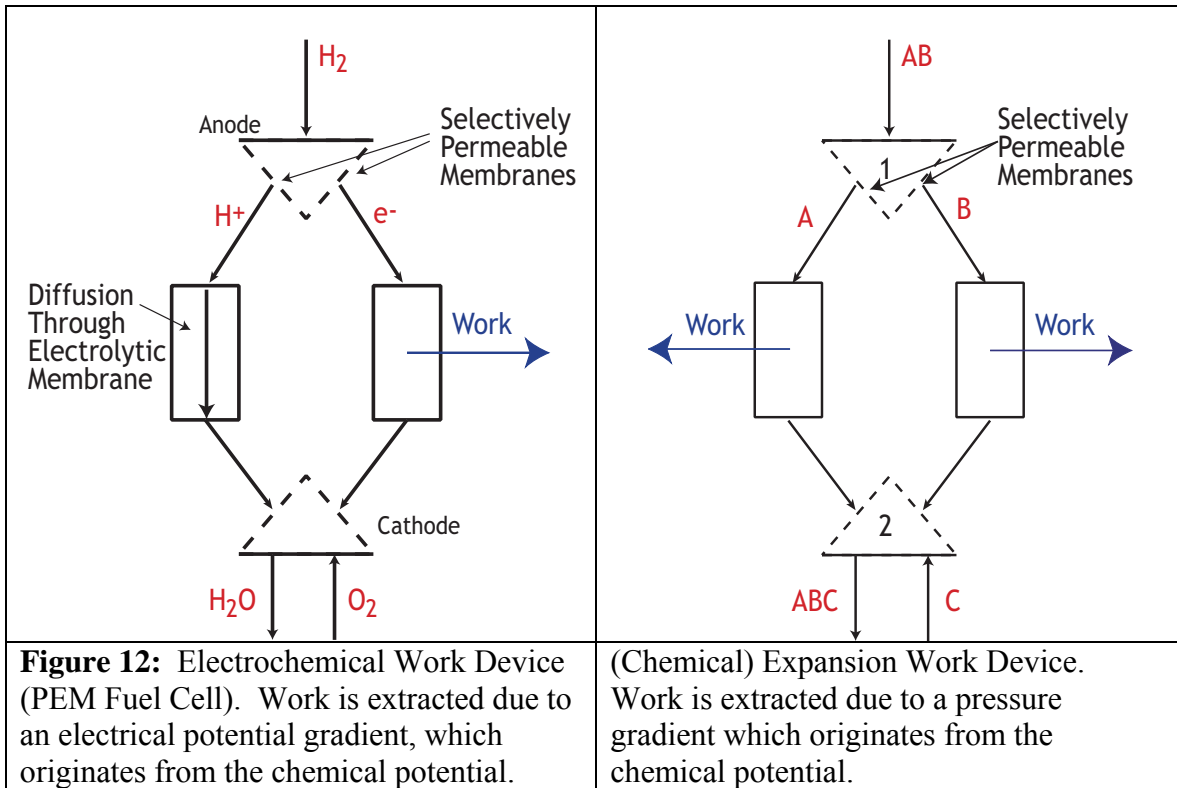
where R is the universal gas constant, T is the temperature, P° is the reference pressure and P_i is the partial pressure of specie i . Assuming, as in the fuel cell, that there is no work extraction from the diffusion of specie A, at equilibrium the partial pressure of species A is a constant everywhere. Only specie B has a partial pressure difference from (1) to (2). Adding $\Delta\mu_1$ and $\Delta\mu_2$ together and solving for $\Delta\mu_{\text{overall}}$ (W_{max}) shows that the maximum work is proportional to the pressure gradient of specie B at constant temperature

$$\Delta\mu_1 + \Delta\mu_2 = \Delta\mu_{\text{tot}} = 0 = \mu_{B1} - \mu_{AB} + \mu_{ABC} - \mu_{B2} - \mu_C$$

$$\mu_{ABC} - \mu_{AB} - \mu_C = \mu_{B2} - \mu_{B1} = RT\ln(P_{B2}/P_{B1}) \text{ at constant } T$$

$$W_{\text{out, max}} = -\Delta\mu_{\text{tot}} = -RT\ln(P_{B2}/P_{B1}) \text{ at constant } T$$

The maximum work possible for an isothermal system (like the fuel cell) is based on the difference in partial pressures between (1) and (2). (Note that $P_{B2} < P_{B1}$ so that the W_{out} is positive.)



A better thermodynamic understanding of the fuel cell will potentially help in designing this expansion work device. The electrochemical potential is a useful property for describing a fuel cell, combining the chemical potential of a species with its electrical potential. Since a fuel cell is a constant temperature and pressure device, the chemical and electrical potentials are the only two driving gradients. The electrochemical potential is defined as

$$\mu_{bar_i} = \mu_i(T, P_i) + z_i F \phi$$

where μ_i is the chemical potential of specie i at T and P_i , z_i is the species charge, F is Faraday's constant, and ϕ is the electrical potential. Since z_i must be nonzero for the second term to contribute, only charged species have an electrical component. For uncharged species such as H_2 , $\mu_{bar_{H_2}} = \mu_{H_2}$.

Knowing the chemical and electrical potential of each species in the fuel cell will give more information about how the fuel cell converts chemical energy directly to electrical energy. At equilibrium, the total change in electrochemical potential is equal to zero at both the anode and the cathode. The chemical reaction at the anode is $H_2(g) \rightarrow 2H^+(aq) + 2e^-(Pt)$ which can be used to write an equation for the total change in electrochemical potential at the anode

$$\Delta\mu_{bar} = 2\mu_{bar_{H^+(aq)}} + 2\mu_{bar_{e^-(Pt)}} - \mu_{bar_{H_2(g)}} = 0$$

Substituting the definition of μ_{bar} and rearranging

$$-2\mu_{H^+(aq)} - 2\mu_{e^-(Pt)} + \mu_{H_2(g)} = 2F(\phi_S - \phi_A)$$

where ϕ_s is the potential of the solution and ϕ_A is the potential of the anode electrode. A similar balance for the cathode reaction ($2\text{H}^+(\text{aq}) + 2\text{e}^-(\text{Pt}) + \frac{1}{2} \text{O}_2(\text{g}) \rightarrow \text{H}_2\text{O}$) yields

$$-\mu_{\text{H}_2\text{O}} + 2\mu_{\text{H}^+} + 2\mu_{\text{e}^-} + 0.5\mu_{\text{O}_2} = 2F(\phi_C - \phi_s)$$

where ϕ_C is the potential at the cathode.

Determining the chemical potential of each species, arbitrarily setting ϕ_A equal to 0, and solving for ϕ_s and ϕ_C provides all the information needed to solve for the electrochemical potentials of each species. $\text{H}_2(\text{g})$, $\text{O}_2(\text{g})$, and $\text{e}^-(\text{g})$ at 298 K are chosen as reference species. Entropy is zero at zero Kelvin. Figure 13 is a plot of μ_i , the chemical potential vs. ϕ_i , the electrical potential for each species. The virtual state for a species represents the magnitude of its total potential; all of the species' electrical potential has been converted to chemical potential. The figure tracks the energy transfers starting with one molecule of H_2 and $\frac{1}{2}$ molecule of O_2 which is why it is necessary to plot 2 protons and 2 electrons. The units for the figure are electron Volts (eV) which are easily converted to a cell potential by dividing by the number of charges. For instance, the two electrons at the cathode have an electrical potential of 2.46 eV which equals the familiar 1.23 V cell potential for a PEM fuel cell.

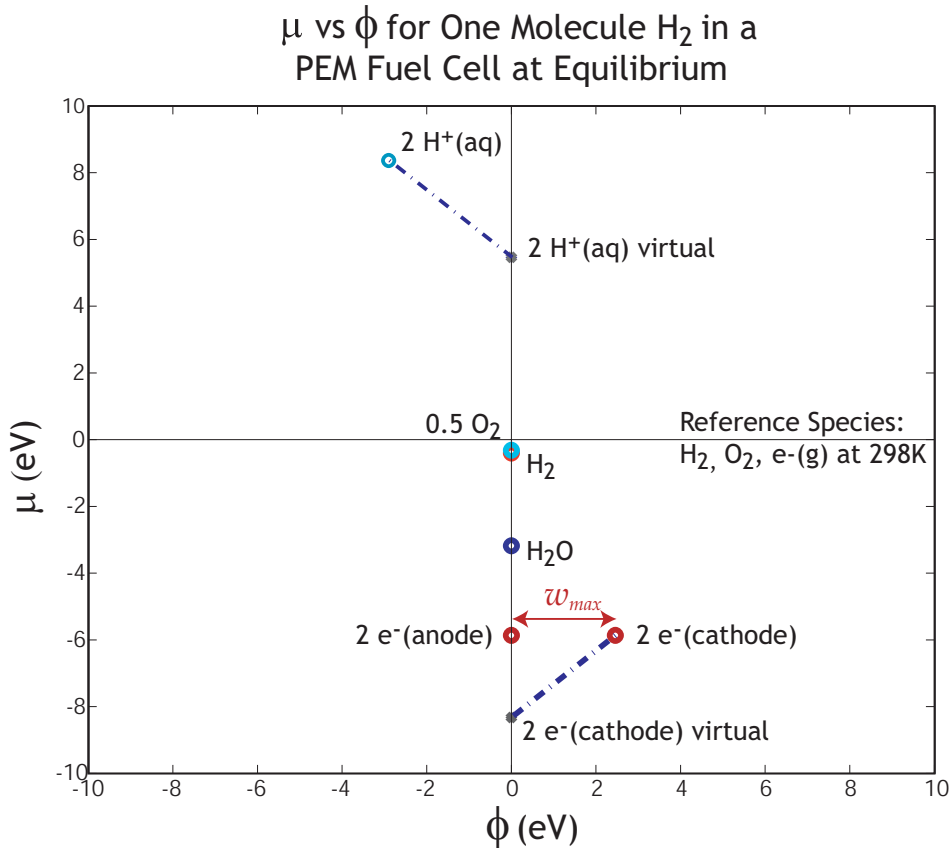


Figure 13: Chemical Potential (μ) vs. Electrical Potential (ϕ) for a PEM fuel cell at equilibrium conditions.

Hydrogen enters the system and is split into low chemical potential electrons and high chemical potential protons. The total electrochemical potential of the protons (shown by the virtual state) is lower than the proton chemical potential because the protons have moved to a lower electrical potential in the solution. The protons' electrochemical potential is the same across the entire membrane at equilibrium. The electrons' chemical potential is the same at the anode and the cathode since the electrons are always in the conduction band of the platinum. Their electrical potential changes, however, as they move down an electrical gradient to the positively charged cathode. The virtual state for the electrons shows that their lowest potential energy is at the cathode. Work, denoted w , is extracted from the electron motion. At the cathode, the protons, electrons, and oxygen combine to form the final product, water.

A similar figure can be made for the expansion work device, where the axes would be chemical potential vs. partial pressure. By mapping the fuel cell energy transfers, we hope to identify the requirements necessary to make the analogous expansion work device—potentially a reversible expansion engine. Efforts to that end are currently under way.

Progress

The last year has seen significant progress toward defining what is possible in the development of low-irreversibility engines. During the first year of the project, preliminary simulations were performed and possible experimental approaches were assessed. During this second year, we selected the piston-engine system as the experimental focus of our studies and initiated specific efforts to understand and prove what is possible in developing improved engine designs. In the experimental work, we have been able to demonstrate that late-phase combustion can lead to significant improvements in efficiency—as hypothesized—but that this improvement is most likely due to a decrease in heat transfer and not a reduction in combustion irreversibility. At the same time, we have also identified that further significant gains are likely to be possible since the working fluid remains highly energetic.

The observation about the mechanism of efficiency improvement in the experiments was bolstered by numerical simulations for adiabatic combustion with expansion. These showed that for a particular family of expansion profiles and fuels, completion of combustion at minimum volume always gave the highest efficiency (and lowest combustion irreversibility). Perhaps the most important accomplishment this year is the extension and application of the Maximum Principle to this optimal adiabatic, expansion problem. The importance of this result is that it shows that regardless of the dynamics of the system (i.e., the chemical kinetics) the necessary condition for an optimal solution to this problem requires that combustion occurs either at maximum or minimum or zero piston speed. Stated another way, because of the linear dependence of the work output on expansion rate, an extremum in the solution can only occur at the extreme design points of expansion rate. From both experiments and simulations, it appears likely that the optimal solution occurs with zero expansion during combustion, that is, at constant volume. Again, the importance of this proof is that it removes the requirement to search the space of possible dynamics—as was initially done in our numerical simulations.

The other benefit of this proof is that it brings into focus what is required to find an optimal design. That is, a non-linear energy interaction. The most obvious of these is heat transfer, which will be the next step in our analytical work. This step will also bring our analysis work into line with our experimental observations. Moving in this direction is also consistent with our objective to systematically explore the space of optimal design as successive interactions are admitted in the design space.

The other area where significant progress has been made is in exploration of whether it is possible to develop an expansion engine that embodies the low-temperature, high-efficiency attributes of the fuel cell (but with using electrochemical work). Having identified a suitable way to extract energy from the chemical potential of the reactants—adiabatic expansion—we have analyzed the energy processes of the PEM fuel cell system in order to better understand what will be required in the design of such an expansion engine. This has been a challenging exercise—certain characteristics of fuel cells that one might believe would be well known, and that are critical to the type of reverse-engineering approach that we have taken, have turned out to not be known. This is less surprising in hindsight, since these are detailed questions which are not often asked except for the most fundamental reasons. But having resolved these questions, the construction of the chemical-potential/electrical-potential diagram shown in the text is a key step towards understanding how a reversible expansion engine might be designed. Because this is a novel idea with a very high efficiency potential, that goal remains a key stretch target of our research in the next year.

Future Plans

A number of research efforts have been identified throughout the discussion and are currently underway. These include:

- (1) Experiments to expand the range of late-phase HCCI operation and to explore optimal expansion to further increase efficiency.
- (2) Incorporating the effect of heat transfer in the simulation model and the dynamic system analysis used for optimization.
- (3) Investigating the option of allowing heat transfer *within* the system boundary (i.e. regeneration) in a low-irreversibility reactive engine.
- (4) Refining electrochemical potential estimates for the PEM fuel cell, including effects such as hydrogen adsorption on platinum and proton concentration in the membrane.
- (5) Estimating heat transfer and activation energies to better understand the role of the metal catalyst in the PEM fuel cell. This understanding will help in defining the required characteristics for a reversible expansion engine.

References

1. P.A. Caton, A.J. Simon, J.C. Gerdes, and C.F. Edwards, *Residual-effected homogeneous charge compression ignition at a low compression ratio using exhaust reinduction*, Int. J. Engine Res. 4, 163-177, 2003.
2. A. Bejan, *Advanced Engineering Thermodynamics*, Wiley, 2001.
3. L.S. Pontryagin, V.G. Boltyanskii, R.V. Gamkrelidze, E.F. Mishchenko, *The Mathematical Theory of Optimal Processes*, Gordon and Breach, New York, 1986.
4. G. Leitmann, *The Calculus of Variations and Optimal Control*, Plenum Press, New York, 1981.
5. R.F. Hartl, S.P. Sethi, R.G. Vickson, *A survey of the Maximum Principles for optimal control problems with state constraints*, SIAM Review, 37, 181-218, 1995.

II.4 Project Results: Advanced Combustion

6. J.T. Betts, *Survey of numerical methods for trajectory optimization*, J. Guid. Control Dyn. 21, 193-207, 1998.

Contact

C.F. Edwards: cfe@stanford.edu